Article

Dendritic Mesoporous Organosilica Nanoparticles with Photosensitizers for Cell Imaging, siRNA Delivery and Protein Loading

Haneen Omar [1],* Sara Jakimoska [2,3], Julia Guillot [2,3], Edreese Alsharaeh [1], Clarence Charnay[3] , Frédérique Cunin[3], Aurélie Bessière[3], Jean-Olivier Durand[3], Laurence Raehm [3], Laure Lichon [2], Mélanie Onofre [2] and Magali Gary-Bobo [2]

[1] Alfaisal University, Riyadh, Saudi Arabia; homar@alfaisal.edu, ealsharaeh@alfaisal.edu
[2] IBMM, Univ. Montpellier, CNRS, ENSCM, Montpellier, France
[3] ICGM, Univ. Montpellier, CNRS, ENSCM, Montpellier, France, clarence.charnay@umontpellier.fr, frederique.cuin@enscm.fr, aurelie.bessiere@umontpellier.fr, jean-olivier.durand@umontpellier.fr, laurence.raehm@umontpellier.fr
* Correspondence: homar@alfaisal.edu

Abstract: Dendritic Mesoporous Organosilica Nanoparticles (DMON) are a new class of biodegradable nanoparticles suitable for biomolecules delivery. In order to escape from the endosomes-lysosomes and to deliver biomolecules in the cytoplasm of cells, we studied photochemical internalization (PCI) and photodynamic therapy (PDT) of DMON. We added photosensitizers in the framework of DMON. DMON were also loaded with siRNA or FVIII factor protein. We made four formulations with four different photosensitizers, The photosensitizers allowed to perform imaging of DMON in cancer cells, but the presence of the tetrasulfide bond in the framework of DMON quenched the formation of singlet oxygen. Fortunately one formulation allowed to efficiently deliver proapoptotic siRNA in MCF-7 cancer cells leading to 31% of cancer cell death, without irradiation. For FVIII protein, it was loaded in two formulations with drug loading capacities (DLC) up to 25%. In conclusion DMON are versatile nanoparticles which allowed to load siRNA and to deliver it in cancer cells, and to load FVIII protein with good DLC. Due to the presence of tetrasulfide, it was not possible to perform PDT and PCI.

Keywords: Dendritic Mesoporous Organisilica Nanoparticles; siRNA; FVIII Factor

1. Introduction

Mesoporous Organosilica Nanoparticles (MON), a new class of nanoparticles whose properties are different from that of well-known Mesoporous Silica Nanoparticles (MSN) [1-4] have found applications in many different fields and these nanomaterials have been comprehensively reviewed. [5-15] The applications mainly concern biology, with anti-cancer applications, but environment decontamination [16] and catalysis [15] have also been studied, showing the large field of applications of these nanoparticles. Indeed the presence of the organic part leads to organic-inorganic hybrids materials, [17,18] which are highly interesting due to the synergy between the organic and inorganic parts, which offers new properties and possibilities. Two subclasses of MON are Intricately structured MON (IMON) [19], and Dendritic MON (DMON), which have been very recently reviewed. [20] DMON has been mainly synthesized from bis(triethoxysilyl)ethane or bis(triethoxysilylpropyl)tetrasulfide, using three types of preparation methods. [20] We were interested in preparing DMON for the vectorization of nucleic acids such as siRNA [20] as they possess large pores suitable for this. Furthermore, mRNA vectorization [21] has also been studied and is very efficient. In the course of our studies of photodynamic therapy (PDT) and photochemical internalization (PCI) of siRNA, [22] we were interested in the preparation of bis(triethoxysilylpropyl)tetrasulfide-based DMON for PDT and PCI of siRNA. For this, we covalently attached photosensitizers inside the framework of the DMON. We used three triethoxysilylated

Preprints (www.preprints.org) | NOT PEER-REVIEWED | Posted: 26 May 2023 doi:10.20944/preprints202305.1923.v1

porphyrins and triethoxysilylated chlorin e6 as these photosensitizers proved efficient for PDT/PCI applications. [23] We then functionalized DMON with lysine amino acid in order to complex nucleic acids [24] thanks to multivalence offered by the grafting of lysine in the pores and at the surface of DMON. We also tested the encapsulation of the FVIII factor as a model protein to evaluate the potential of DMON in this field.

2. Results and discussion

First, the 4 commercially available photosensitizers PS1-4 were classically triethoxysilylated following literature procedures respectively [25-28].

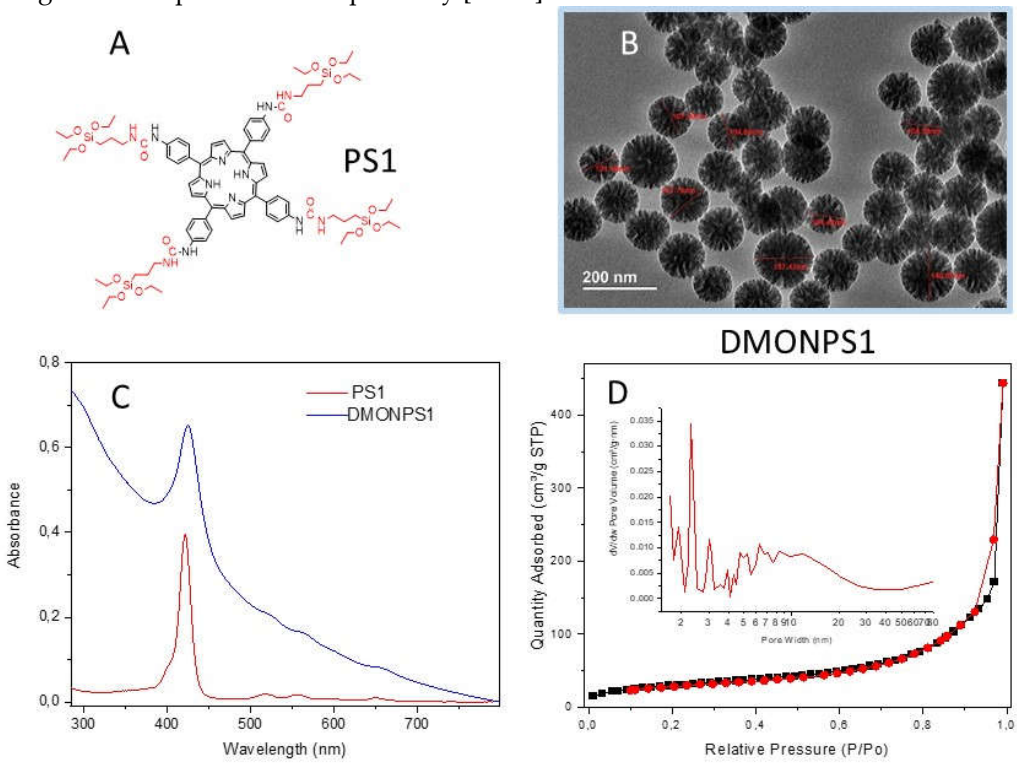

Figure 1. A) The tetraaminophenylporphyrin with four triethoxysilyl groups used for the preparation of DMONPS1. B) DMONPS1 as shown by TEM, the dendritic structure is visible. C) UV-Vis spectra in EtOH of the silylated photosensitizer(PS1) and the corresponding DMONPS1, the photosensitizer is encapsulated inside the framework of DMONPS1, the Soret and four Q bands are visible. D) Nitrogen adsorption–desorption at 77 K (BET). Insert BJH adsorption (dV/dw) Pore Volume.

Preprints (www.preprints.org) | NOT PEER-REVIEWED | Posted: 26 May 2023 doi:10.20944/preprints202305.1923.v1

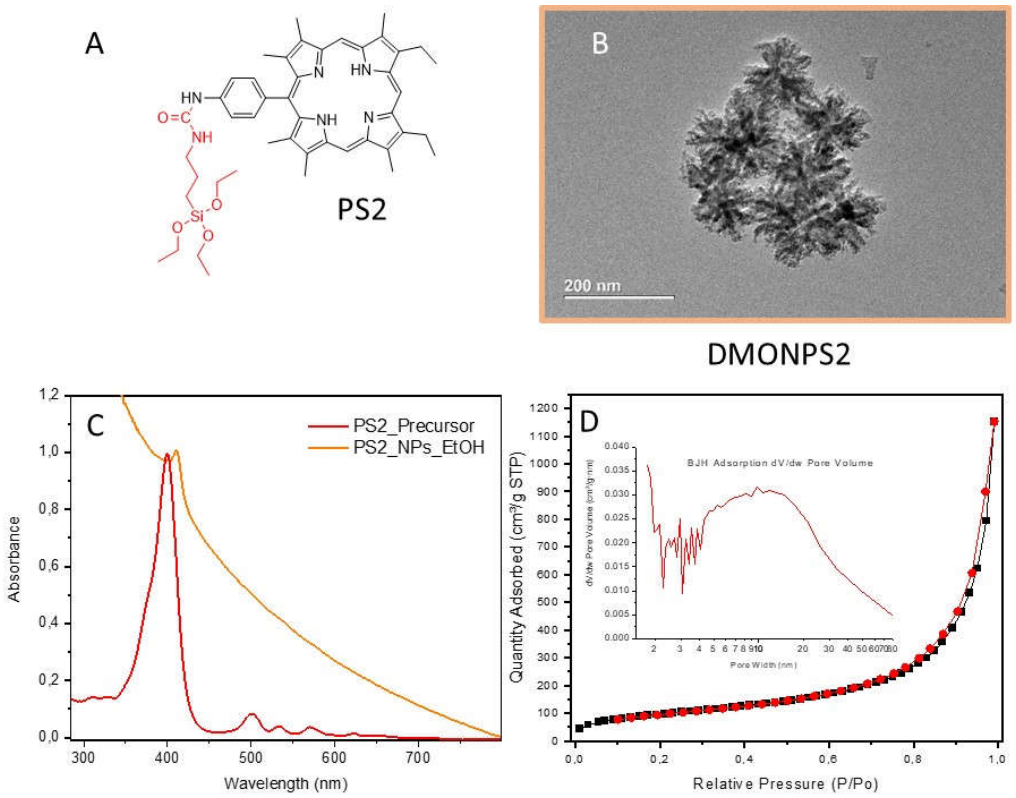

Figure 2. A) The monosilylated aminophenylporphyrin used for the preparation of DMONPS2. B) DMONPS2 as shown by TEM, the dendritic structure is visible, the nanoparticles seem aggregated. C) UV-Vis spectra in EtOH of the silylated photosensitizer(PS2) and the corresponding DMONPS2, the photosensitizer is encapsulated inside the framework of DMONPS2, the Soret band is visible. D) Nitrogen adsorption–desorption at 77 K (BET). Insert BJH adsorption (dV/dw) Pore Volume.

Preprints (www.preprints.org) | NOT PEER-REVIEWED | Posted: 26 May 2023 doi:10.20944/preprints202305.1923.v1

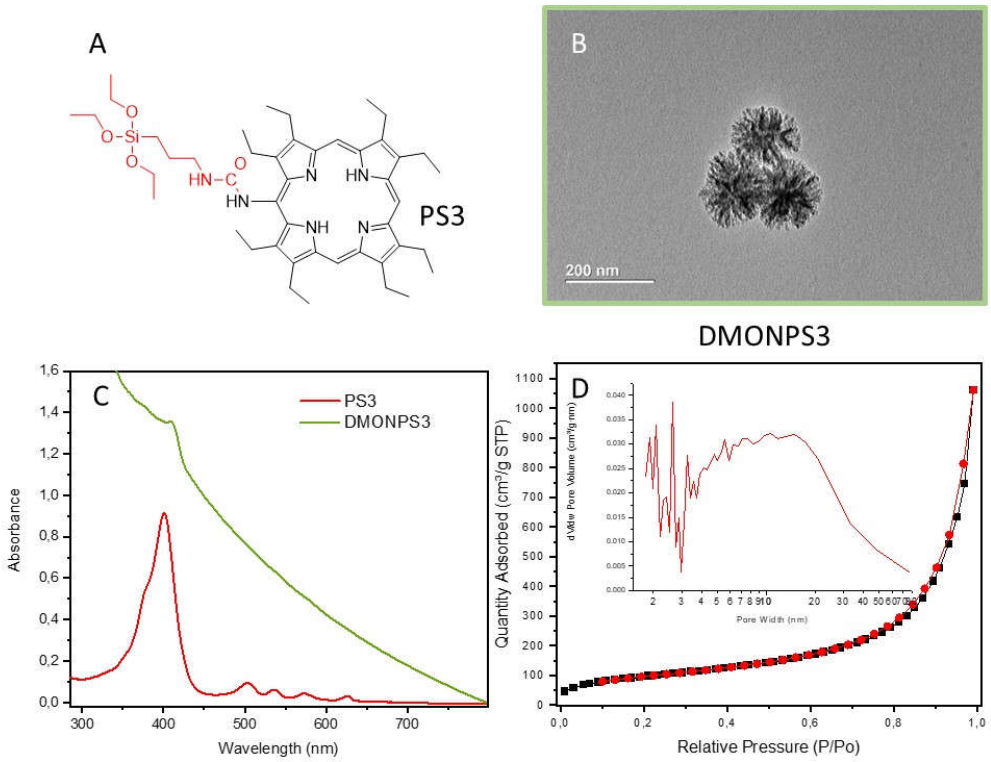

Figure 3. A) The monosilylated aminoporphyrin used for the preparation of DMONPS3. B) DMONP3 as shown by TEM, the dendritic structure is visible. C) UV-Vis spectra in EtOH of the silylated photosensitizer(PS3) and the corresponding DMONPS3, the photosensitizer is encapsulated inside the framework of DMONPS3, the Soret band is visible. D) Nitrogen adsorption–desorption at 77 K (BET). Insert BJH adsorption (dV/dw) Pore Volume.

Preprints (www.preprints.org) | NOT PEER-REVIEWED | Posted: 26 May 2023 doi:10.20944/preprints202305.1923.v1

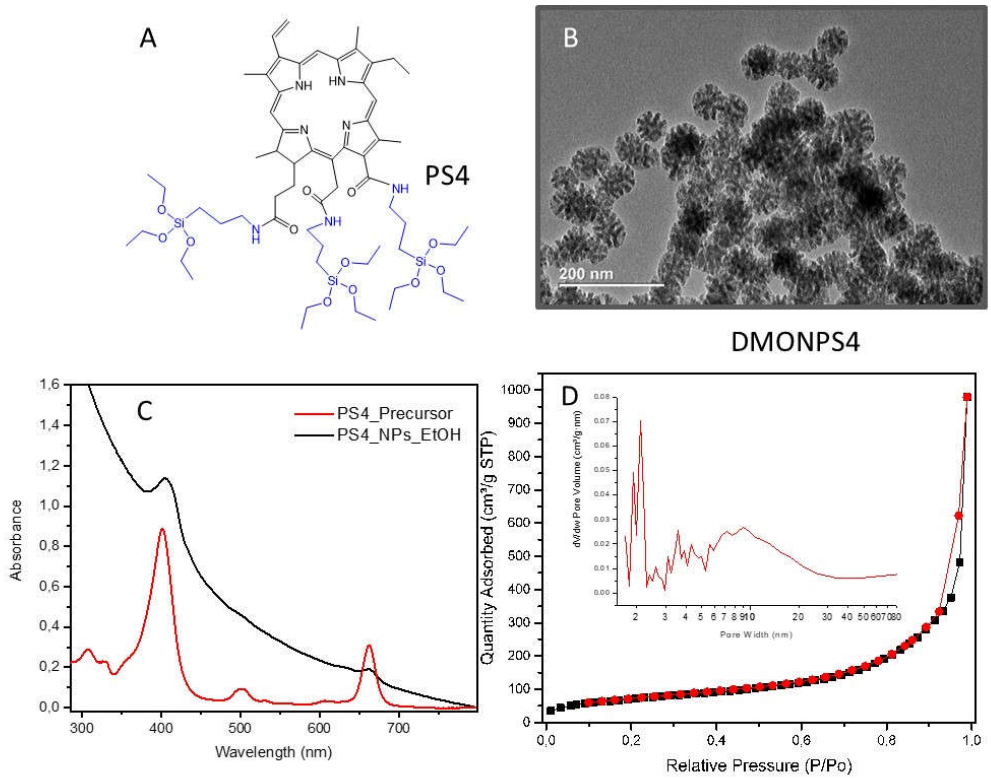

Figure 4. A) The trisilylated chlorin e6 used for the preparation of DMONPS4. B) DMONP4 as shown by TEM, the dendritic structure is visible. C) UV-Vis spectra in EtOH of the silylated photosensitizer(PS4) and the corresponding DMONPS4, the photosensitizer is encapsulated inside the framework of DMONPS4, the Soret and Q1 bands are visible. D) Nitrogen adsorption–desorption at 77 K (BET). Insert BJH adsorption (dV/dw) Pore Volume.

DMON-PS1-4 were then prepared by mixing the corresponding triethoxysilylated photosensitizers (**Figure 1A, 2A, 3A, 4A**) in the presence of tetraethoxysilane, bis(triethoxysilylpropyl)tetrasulfide, following a one-pot known procedure using NaSal (sodium salicylate) and cationic surfactant CTAB as structure directing agents and triethanolamine as a catalyst. [29] The dendritic structure and the presence of radial mesopores were clearly shown with transmission electron microscopy (TEM) (**Figure 1B, 2B, 3B, 4B**) of DMONPS1-4. DLS showed well-dispersed nanoparticles from 95-100 nm, hydrodynamic diameters in agreement with TEM images. The photosensitizers were clearly incorporated inside the structure of DMONPS1-4 as shown by UV-Vis spectra. (**Figure 1C, 2C, 3C, 4C**). With PS1 possessing four triethoxysilyl groups, the Q bands were visible after incorporation in DMONPS1 despite light scattering, which was not the case for DMONPS2, DMONPS3 due to a lower amount of incorporation. The Q1 band was present for the chlorin e6 derivative (DMONPS4) showing that the structure was not damaged during the mild sol-gel method used for the preparation of the nanoparticles. N_2 adsorption-desorption was studied for all the DMONPS. (**Figure 1D, 2D, 3D, 4D, Table 1**). All the nanoparticles showed type IV isotherms. The Brunauer–Emmett–Teller (BET) surface area and the total pore volume of DMONPS1 were 110 $m^2.g^{-1}$ and 0.44 $cm^3.g^{-1}$ respectively. The capillary condensation step occurred in the relative pressure (P/P0) of 0.8–0.9, corresponding to a large pore size of ~24.4 nm (inset of **Figure 1D**). Interestingly, with DMONPS2 and DMONPS3, the BET-specific surface area increased to 356, 353 $m^2.g^{-1}$, with an increase of the pore volumes to 1.78, 1.65 $cm^3.g^{-1}$ and a decrease of the pore size to 19.5 and 18.2 nm respectively. The structure of DMONPS4 was between DMONPS1 and DMONPS2-3 with a BET-specific surface area of 266 $m^2.g^{-1}$ a pore volume of 1.52 $cm^3.g^{-1}$ and a pore size of 22.6 nm. In order to complex siRNA, functionalization of DMONPS1-4 with lysine (**Scheme 1**), by amination with aminopropyltriethoxysilane (APTES), coupling with protected lysine, and deprotection was then performed. DMONPS1-4 showed a negative zeta potential in agreement with the deprotonation of

Preprints (www.preprints.org) | NOT PEER-REVIEWED | Posted: 26 May 2023 doi:10.20944/preprints202305.1923.v1

Si-OH in water. After amination, the zeta potential turned positive (**Table 1**) and after functionalization with lysine, high zeta potential values were observed indicating that the functionalization was successful, except for DMONNPS4-Lys.

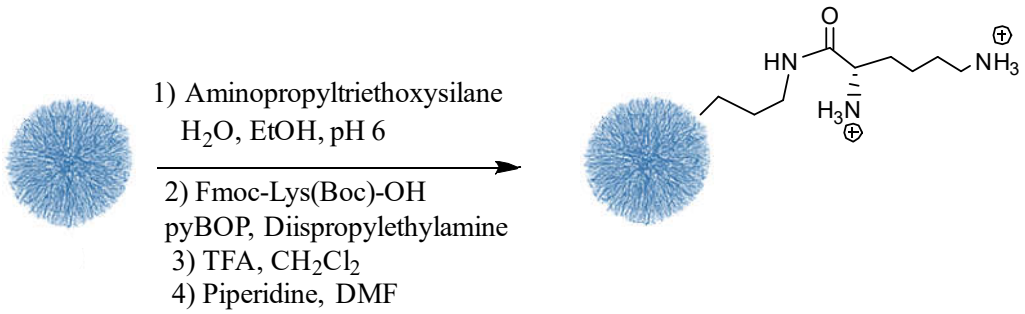

Scheme 1. Functionalization of DMONPS1-4 with lysine amino acid (DMONPS1-4-Lys) in order to complex siRNA.

Table 1. Data for DMON.

DMONPS	DLS (nm)	ZETA Potential (mV)	BET ($m^2.g^{-1}$)	Pore size (nm)	Pore volume $cm^3.g^{-1}$
DMONPS1	100	-8.1	110	24.4	0.44
DMONPS2	92	-8.5	356	19.5	1.78
DMONPS3	96	-10.4	353	18.2	1.65
DMONPS4	95	-7.5	265	22.6	1.52
DMONPS1-NH_2	100	6.0	/	/	/
DMONPS2-NH_2	99	4.8	/	/	/
DMONPS3-NH_2	100	5.1	/	/	/
DMONPS4-NH_2	100	6.3	/	/	/
DMONPS1-Lys	99	42.0	/	/	/
DMONPS2-lys	99	26.3	/	/	/
DMONPS3-Lys	100	26.4	/	/	/
DMONPS4-Lys	100	6.0	/	/	/

The nanoparticles were then incubated with cancer cells for 24 h, at a concentration of 50 $\mu g.mL^{-1}$, which was adequate for imaging, and confocal microscopy was performed (**Figure 5**). The nanoparticles were excited at 420 nm, in the Soret band of the porphyrin and chlorin.

Preprints (www.preprints.org) | NOT PEER-REVIEWED | Posted: 26 May 2023 doi:10.20944/preprints202305.1923.v1

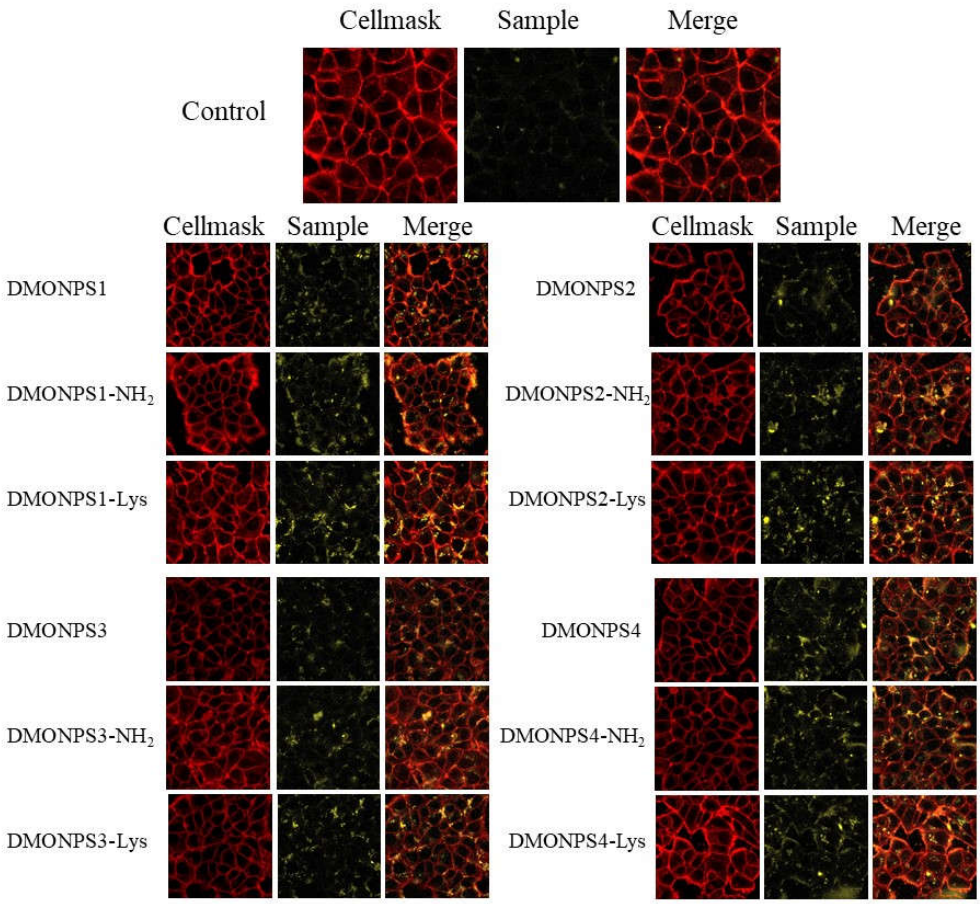

Figure 5. Confocal microscopy imaging of MCF-7 cancer cells incubated with DMONPS1-4, DMONPS1-4-NH_2 or DMONPS1-4-Lys, for 24h. $\lambda_{excitation}$ = 420 nm $\lambda_{emission}$ = 630-670 nm. Membranes were stained with a cell mask 15 Min. before observation. $\lambda_{excitation}$ = 561 nm $\lambda_{emission}$ = 565-629 nm.. .

All the nanoparticles were endocytosed by MCF-7 cells, but DMONPS1-4-NH_2 and DMONPS1-4-Lys with positive zeta potential were more endocytosed in the cells, in agreement with a stronger interaction of the positive charge with the cell membrane.

Preprints (www.preprints.org) | NOT PEER-REVIEWED | Posted: 26 May 2023 doi:10.20944/preprints202305.1923.v1

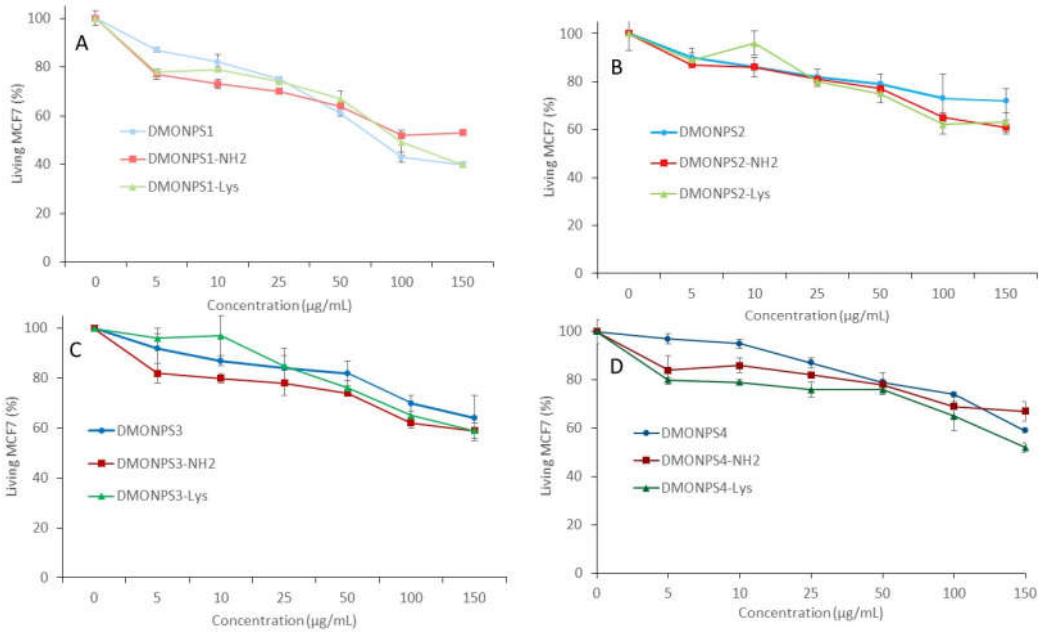

Figure 6. Cytotoxicity studies of MCF-7 cancer cells were performed through incubation with DMONPS1-4, DMONPS1-4-NH_2 or DMONPS1-4-Lys, for 72h. The cytotoxicity was monitored with the MTT assay.

Cytotoxicity studies were then performed (**Figure 6**). 25 µg.mL^{-1} was the adequate concentration to carry out photodynamic therapy (PDT) experiments as the nanoparticles presented low toxicity above 75% after three days. The cells were classically irradiated [26] at 405 nm in the Soret band, for 5 min. or at 650 nm for 20 min. in the QI band, but PDT effects were not observed (data not shown). Indeed we believe that the tetrasulfide group quenches the formation of singlet oxygen through oxidation. [30] The photosensitizers allow only imaging of cancer cells.

Complexation of DMONPS1-4-Lys with siRNA (Inhibitor Apoptotic Protein) IAP was then performed (**Figure 7**) and monitored with a gel retardation assay. Proapoptotic siRNA would inhibit the production of anti-apoptotic proteins, with the activation of the apoptotic pathway, leading to cell death. A very good complexation was noticed at concentrations of 1/25 for DMONPS1-2-lys, and 1/10 for DMONPS3-4-lys.

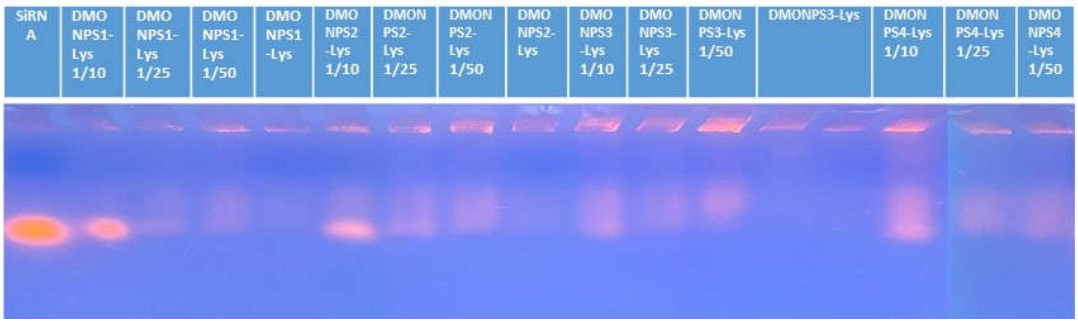

Figure 7. Agarose gel-retardation assay with DMONPS1-4-Lys, complexed with siRNA (negative control (A)), at different weight ratios ranging from 1/10 to 1/50. Electrophoresis was immediately performed after complex formation for 30 min at 37 °C.

After having determined the complexation of the siRNA/nanoparticles ratio, we then investigated the siRNA IAP delivery in MCF-7 breast cancer cells (**Figure 8**). We incubated the DMONPS1-4-Lys-siRNA complexes or siRNA alone with MCF-7 cancer cells for three days. MTT assay was carried out to monitor the siRNA effect (**Figure 8**).

Preprints (www.preprints.org) | NOT PEER-REVIEWED | Posted: 26 May 2023 doi:10.20944/preprints202305.1923.v1

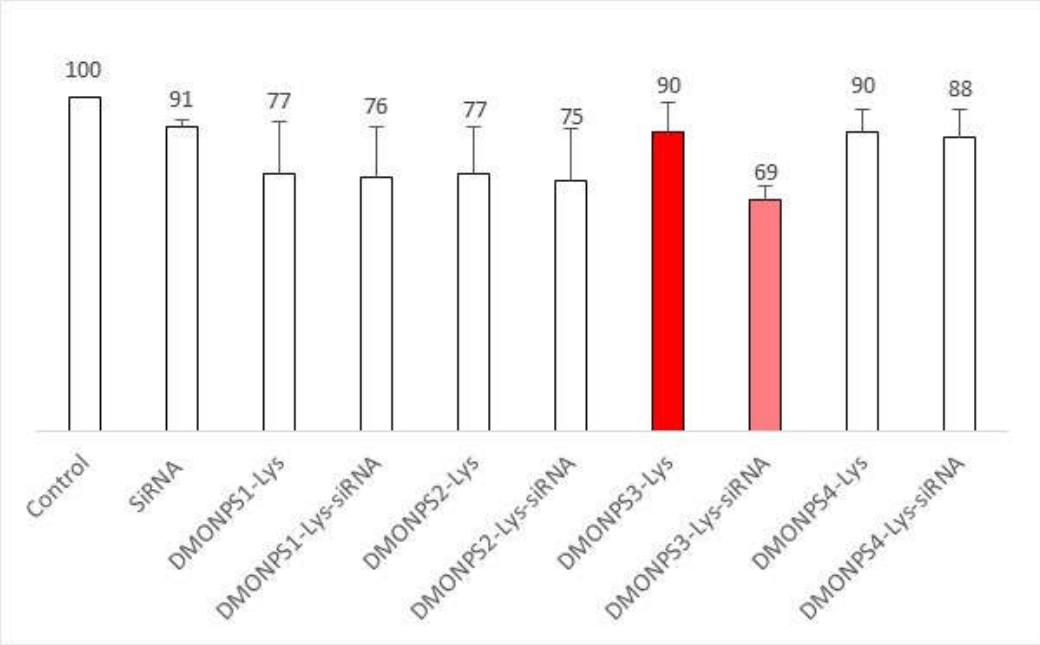

Figure 8. Anticancer effect of DMONPS1-4 complexed with siRNA inhibitor of apoptosis protein (IAP). MCF-7 cells were treated (or not) with free DMONPS1-4 (at 25 µg.mL^{-1}) or DMONPS1-4 complexed with siRNA at a 1/15 ratio. The killing effect was monitored with the MTT assay.

None of the nanoparticles were able to deliver the siRNA except DMONPS3-Lys. DMONPS3-Lys led to 90% MCF-7 survival whereas DMONPS3-Lys-siRNA led to 31% of cancer cell death. This result could be explained by the structure of the nanoparticles. BET analysis showed that DMONPS3 possess a high specific surface area with pore size suitable for siRNA encapsulation, furthermore, they were not aggregated with a hydrodynamic diameter suitable for the delivery of siRNA in the cytoplasm of the cells. We suggest that the high level of GSH in the cytoplasm of cancer cells allowed delivery of siRNA through cleavage of the tetrasulfide link present in the structure of the DMONPS3-Lys-siRNA complex.

After that, we tested the encapsulation of the FVIII protein factor as a model protein, in DMONPS1-Lys and DMONPS3-Lys. FVIII factor is a protein that plays a crucial role in blood clotting. [31] It is produced in the liver and circulates in the blood. FVIII deficiency is the cause of hemophilia A, a genetic bleeding disorder Hemophilia A patients require regular infusions of FVIII to prevent bleeding episodes. FVIII is administered intravenously. The half-life of FVIII in the body is approximately 8-12 hours. Therefore, encapsulation of FVIII could be of high interest. Furthermore, the global charge of factor VIII is negative. This is because FVIII is a glycoprotein, [32] and the carbohydrate component contains negatively charged molecules, such as sialic acid and sulfate groups, which contribute to the overall negative charge of the protein.

Table 2. Data for the encapsulation of FVIII factor in DMONPS1-Lys and DMONPS3-Lys.

DMONPS	DLC 2 mg/mL FVIII	DLE 2 mg/mL FVIII	DLC 4 mg/mL FVIII	DLE 4 mg/mL FVIII
DMONPS1-Lys	14 %	40 %	/	/
DMONPS3-Lys	12%	35%	25%	42%

We tested the encapsulation of FVIII in DMONPS1,3-Lys. DLC and DLE at 2 mg/mL of protein in PBS were quite interesting with 12-14% of loading and 35-40% of DLE. By increasing the amount of protein in the feeding solution, higher DLC was reached with DMONPS3-Lys up to 25% of DLC.

Preprints (www.preprints.org) | NOT PEER-REVIEWED | Posted: 26 May 2023 doi:10.20944/preprints202305.1923.v1

3. Materials and Methods

The following chemicals, cetyltrimethylammonium bromide (CTAB), sodium salicylate (NaSal), tetraethyl orthosilicate (TEOS), bis[3-(triethoxysilyl)propyl]tetrasulfide (BTES), triethanolamine (TEA), ammonium nitrate (NH_4NO_3), ethanol (EtOH), dichloromethane (DCM), N,N-Diisopropylethylamine (DIPEA), isocyanatopropyltriethoxysilane, anhydrous tetrahydrofuran (THF), ethylacetate (AcOEt) and recrystallized in hexane, dimethyl sulfoxide (DMSO), (3-Aminopropyl)triethoxysilane (APTES), carbodiimide hydrochloride (EDC-HCl) and N-hydroxysuccinimide (NHS), were purchased from Sigma-Aldrich. 5,10,15,20-meso-tetra(4-aminophenyl)porphyrin and 2,3,7,8,12,13,17,18-octaethylporphyrin-5-amine were purchased from TCI. 5-(4-aminophenyl)-2,3,7,8,12,18-(hexamethyl)-13,17-(diethyl)porphyrin was purchased from Porphychem. Conjugated chlorin e6 (Ce6) was purchased from Frontier Scientific. FVIII factor was purchased from Merck.

3.1. Silylation of PS1-4

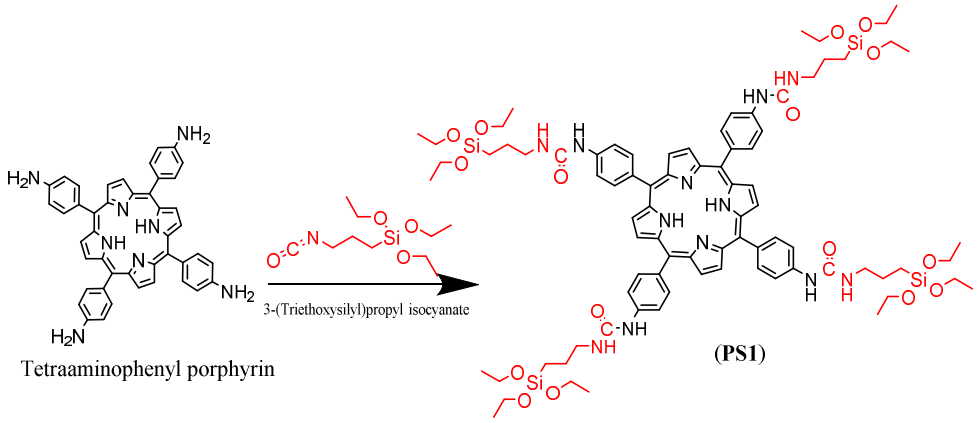

Firstly, a mixture of 5,10,15,20-meso-tetra(4-aminophenyl)porphyrin (200 mg,(0.3mmol) 1.4*10-2 mmol), DIPEA (11.2 mg), isocyanatopropyltriethoxysilane (362.8 mg (1.47mmol)) was stirred in anhydrous THF (7 mL) under argon at 80°C overnight (Scheme 1). After evaporation of the solvent, the POR precursor was washed with AcOEt and recrystallized in hexane. This process was repeated 4 times. Finally, the precursor was dried under vacuum. 1H NMR (300 MHz, DMSO-d6) was done to prove the silylation of the porphyrin (Figure). (δ (ppm) 8.88 (s, 8H, Hβpyrrole), 8.86 (s, 4H,CO-NH-CH_2), 8.06 (d, 3 J=9.0 Hz, 8H, H3,5 aryl), 7.84 (d, 3 J=9.0 Hz, 8H, H2,6 aryl), 6.40 (t, 4H, 3 J=4.5 Hz, CO-NH-Ph), 3.81 (q, 3 J=7.5 Hz, 24H, O-CH_2-CH_3), 1.20 (t, 3 J= 7.5 Hz, 36H, O-CH_2-CH_3), 0.66 (t, 3 J=9.0 Hz, 8H, CH_2-Si)

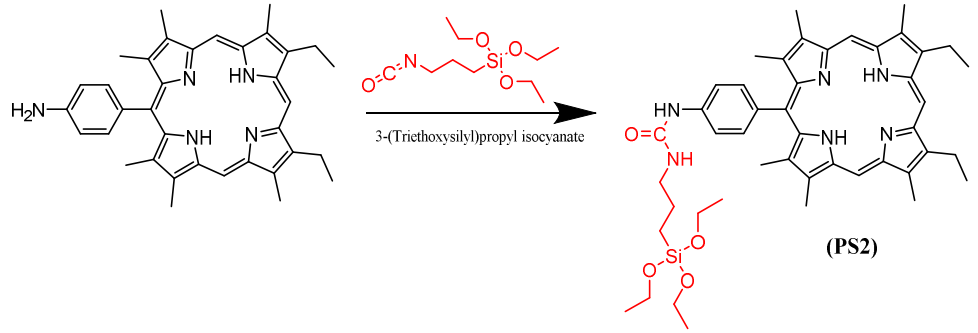

Table 5. aminophenyl)-2,3,7,8,12,18-(hexamethyl)-13,17-(diethyl)porphyrin precursor (25 mg, 0.0456 mmol) in anhydrous THF (7 mL) and DIPEA (0.015 mL, 11.2 mg,), 3-isocyanatopropyltriethoxysilane (17 mg, 17 µl, 0.0684 mmol) was slowly added, and the mixture was stirred under argon at 80°C overnight. Volatiles were evaporated.

Preprints (www.preprints.org) | NOT PEER-REVIEWED | Posted: 26 May 2023 doi:10.20944/preprints202305.1923.v1

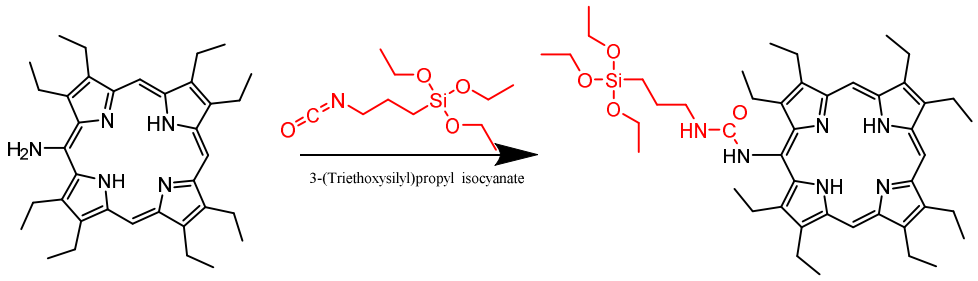

(PS3)

To a solution of 2,3,7,8,12,13,17,18-octaethylporphyrin-5-amine precursor (25 mg, 0.0455 mmol) in anhydrous THF (7 mL) and DIPEA (0.015 mL, 11.2 mg,), 3-isocyanatopropyltriethoxysilane (17 mg, 17 µl, 0.0684 mmol) was slowly added, and the mixture was stirred under argon at 80°C overnight. Volatiles were evaporated.

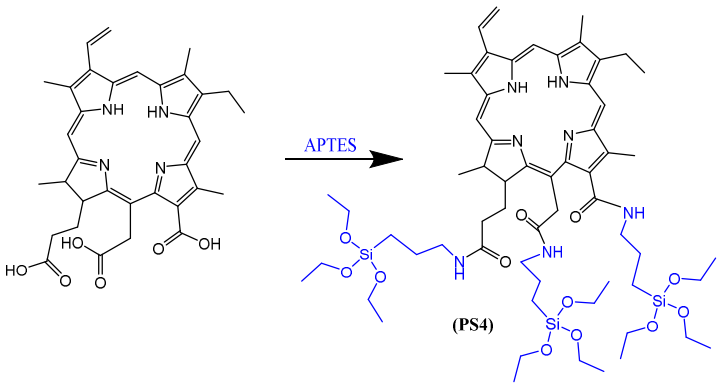

(PS4)

2.2 mg of conjugated chlorin e6 (Ce6) pre-dissolved in 0.5 mL of DMSO were mixed with 12 µL of APTES, in the presence of 6 mg of EDC-HCl, and 4 mg of NHS. The mixture was stirred overnight at room temperature.

3.2. Preparation of DMONPS1-4

DMONPSs were synthesized via a one-pot synthesis using NaSal and cationic surfactant CTAB as structure-directing agents, TEOS and BTES as a silica source, and TEA as a catalyst. The synthesis was conducted in a 50 mL flat-bottom glass bottle with a stirring bar of 3 cm. In a typical synthesis of DMONs, 0.034 g of TEA was added to 12.5 mL of water and stirred gently (~700 rpm) at 80 °C in an oil bath under a magnetic stirrer for 0.5 h. Afterward, 190 mg of CTAB and 42 mg of NaSal were added to the above solution, which was kept stirred for another 1 h. After CTAB and NaSal were completely dissolved, a mixture of 1 mL of TEOS (Mw: 208.33,0.0048 mmol) and 0.8 mL of BTES (Mw: 538.95, 0.00148 mmol) and PS (25 mg for PS1-3, 2.5 mg for PS4) was added to the water–CTAB–NaSal–TEA solution with vigorous stirring for 12 h. The product was recovered by centrifugation of 20 000 rpm for 5 min and washed with ethanol three times to remove the residual reactants. Finally, the yellow powder was dried in a vacuum oven at 40 °C for 6 h. Then, the collected products were extracted with HCl and methanol solution 6g/L NH_4NO_3 solution in 95 % EtOH at 60 °C for 6 h three times to remove the template, followed by drying in vacuum at room temperature overnight.

3.3. Preparation of DMONPS1-4 -NH2

100 mg DMONPS were suspended with 110 mL EtOH for 10 min. 2,4 mL H_2O and 155 uL APTES were added. The pH was adjusted to 6 by the addition of HCl. The reaction was stirred at 750 rpm at r.t. for 20 h. The nanoparticles were centrifuged and washed (X3) with EtOH and then dried under vacuum.

Preprints (www.preprints.org) | NOT PEER-REVIEWED | Posted: 26 May 2023 doi:10.20944/preprints202305.1923.v1

3.4. Preparation of DMONPS1-4- Lys

20 mg of PS NPs-NH_2 were suspended in 2 mL of EtOH. 30 mg of Fmoc-Lys(Boc)-OH was added with 35 mg of PyBOP and 11 µL of DIPEA The suspension was stirred for 18 h at r.t. The nanoparticles were centrifuged then washed with EtOH, and treated with TFA/DCM solution (2 mL, 1:1) for 3 min at r.t. After washing (X3)with EtOH, Fmoc deprotection was performed by adding a solution of Piperidine/DMF (2 mL, 1:1) for 30 min with sonication. After centrifugation for 15 min at 14000 rpm, the supernatant was collected and used for UV-Vis spectroscopy at 290 nm wavelength.

4. Biological studies

4.1. Cell culture

MCF-7 was obtained from human breast cancer cells. MCF-7 were cultured in Dulbecco's Modified Eagle Medium (DMEM) medium supplemented with 10% FBS and 1% penicillin/streptomycin. MCF-7 was allowed to grow at 37°C in a humidified atmosphere under 5% of CO2.

4.2. Cytotoxicity study

MCF-7 cells were seeded into a 96-well plate, 2000 cells per well in 200 µL of culture medium and allowed to grow for 24 hours. Samples become soluble on ethanol absolute at 5 mg/mL.

Twenty hours after seeding, MCF-7 was treated with increasing concentrations from 5 to 150 µg/mL of nano. Three days after the treatment a MTT assay was performed to determine the cell viability. Briefly, cells were incubated for 4 hours with 0.5 mg/mL of MTT (3-(4,5-dimethylthiazol-2-yl)-2,5-diphenyltetrazolium bromide) in media. The MTT/media solution was then removed and the precipitated crystals were dissolved in ethanol/DMSO (v/v). The solution absorbance was read at 540 nm in a microplate reader.

4.3. Confocal Fluorescent Imaging on MCF-7

Confocal fluorescent imaging was performed on MCF-7 cells seeded onto glass bottom dishes at 60 000 cells per well in 1 mL of culture medium and allowed to grow for 24 h. Then cells were incubated for 24 h with or without nanoparticles at 50 µg.mL-1 for each sample. After 24 hours the incubation of cells with CellMask was performed for cell membrane staining for 15 min and cells were washed 3 times with PBS. Fluorescence pictures were recorded on a confocal microscope (LSM 880 Zeiss Microscope) under a 420 nm wavelength excitation for nanoparticle detection and a 561 nm for cell membrane imaging.

4.4. Gel Electrophoresis with siRNA

A total of 5 µL of a 20 µM siRNA, mixed with the appropriate amounts of nanoparticles (in order to reach the desired P+/P- ratio) in RNase-free water (final volume: 20 µL) was used to perform gel retardation assays with siRNA and 4 µL of Blue 6X loading dye (Fisher Scientific, Hampton, NH, USA) was then added. These samples were submitted to electrophoresis performed with a 2% wt/vol agarose gel in TBE (90 mM Tris-borate/2 mM EDTA, pH 8.2) at 50 V for 1 h. The standard was a 100 bp DNA ladder (Sigma-Aldrich, Saint-Quentin-Fallavier, France). To visualize siRNA, a GelRed nucleic acid gel stain (Interchim, Montluçon, France) was used allowing to detect siRNA through an ultraviolet transilluminator (Infinity Gel documentation Imaging, Vilber Lourmat, Paris, France).

4.5. In vitro siRNA Delivery

MCF-7 cells were seeded in a 96-well plate at 2000 cells per well in a 100 µL culture medium. Twenty-four hours after, the cells were incubated with or without NP or NP/siRNA at a ratio of 1/15. Three days after, cells were submitted to MTT assay as described previously. The siRNA is a siRNA IAP, targeting sequence is Inhibitor Apoptotic Protein (siCIAP1) 5'-CUAGGAGACAGUCCUAUUCdTdT-3'. It was purchased from Eurogentec (Serring, Belgium).

Preprints (www.preprints.org) | NOT PEER-REVIEWED | Posted: 26 May 2023 doi:10.20944/preprints202305.1923.v1

4.6. FVIII encapsulation

For the encapsulation of FVIII in DMONPSI-Lys, 5 mg of powdered nanoparticles were mixed with 5 mL of FVIII previously diluted in PBS (10mM, pH 7.4) to obtain a final concentration of 2 mg/mL. For the encapsulation of FVIII in DMONPS3-Lys, two batches of 5 mg of powdered nanoparticles were mixed with 5 mL of FVIII previously diluted in order to have final concentrations of 2 mg/mL or 4 mg/mL. To suspend the solution, a sonication of 5 seconds was carried out then the solution was incubated at room temperature at 200 rpm for 24 hours

$$\text{DLC (\%)} = \frac{\text{Mass of FVIII in the DMONPS1,3-Lys}}{\text{Mass of DMONPS1,3-Lys}}$$

$$\text{DLE (\%)} = \frac{\text{Mass of FVIII in the DMONPS1,3-Lys}}{\text{Mass of FVIII in the feeding solution}}$$

DLC and DLE were calculated after centrifugation and titration of the supernatant with UV-Vis spectra at 280 nm, using two calibration curves.

Calibration curves were determined at 2 mg/mL and 4 mg/mL of FVIII respectively

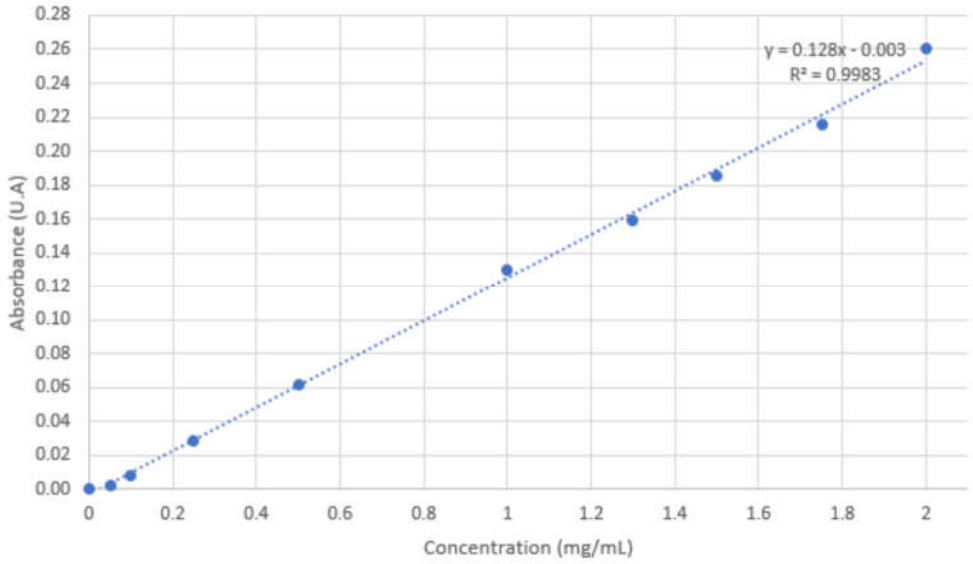

Figure 9. Calibration curve of FVIII at 2 mg/mL in PBS.

 doi:10.20944/preprints202305.1923.v1

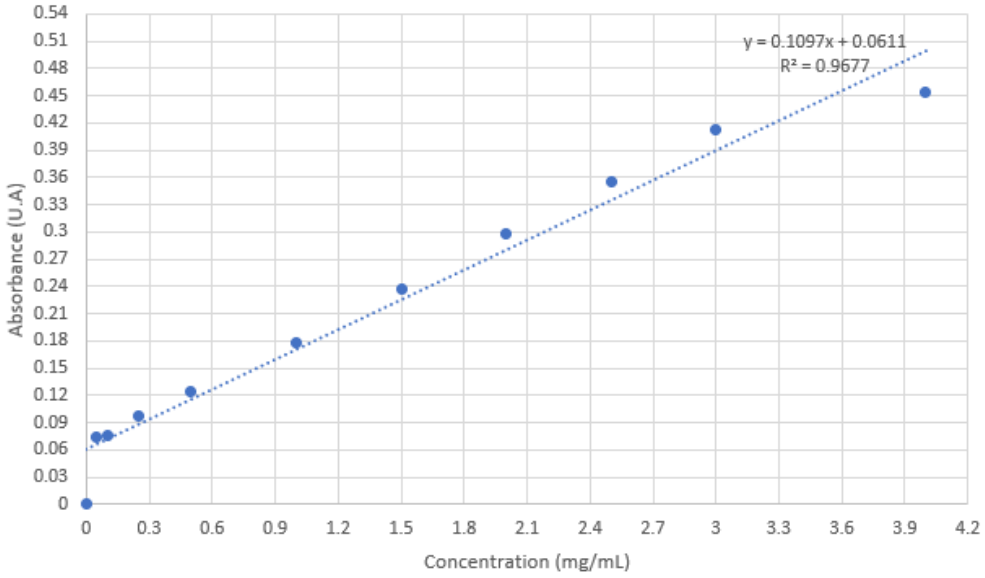

Figure 10. Calibration curve of FVIII at 4 mg/mL in PBS.

5. Conclusions

We have prepared four dendritic mesoporous organosilica nanoparticles with photosensitizers inside and these nanoparticles were then functionalized with lysine in order to first complex siRNA. Unfortunately, photodynamic therapy and photochemical internalization were unsuccessful because of the presence of the tetrasulfide bridge, which quenches singlet oxygen production. However, one formulation proved efficient for the delivery of siRNA IAP in cancer cells, as the structure of these nanoparticles was probably suitable for this purpose. Furthermore loading of FVIII factor in two preparations was efficient with high DLC and DLE. Therefore, the versatility of DMON could be very useful for further nanomedicine applications and personalized medicine.

Author Contributions: Conceptualization, J.-O. D., C.C. and A.B.; methodology, H.O., S.J., J.G., E.A., L.L., M.O.; validation, F.C. and L.R.; formal analysis, L.R., E.A.; investigation, H.O., S.J., J.G., E.A., L.L., M.O.; writing—original draft preparation, J.-O.D., H.O., F.C.; writing—review and editing, A.B., F.C., H.O.; supervision, J.-O.D., L.R., C.C., M.G.-B.; All authors have read and agreed to the published version of the manuscript."

Funding: This research received no external funding.

Data Availability Statement: In this section, please provide details regarding where data supporting reported results can be found, including links to publicly archived datasets analyzed or generated during the study. Please refer to suggested Data Availability Statements in section "MDPI Research Data Policies" at https://www.mdpi.com/ethics. If the study did not report any data, you might add "Not applicable" here.

Acknowledgments: Rio imaging platform at CNRS is gratefully acknowledged. S.J. and J.G. thank Master Ingénierie Biomoléculaire et Nanobiotechnologies (IBION-TEC).

Conflicts of Interest: The authors declare no conflict of interest.

References

1. Manzano, M.; Vallet-Regi, M. Mesoporous silica nanoparticles for drug delivery. *Adv. Funct. Mater.* **2019**, 10.1002/adfm.201902634, Ahead of Print, doi:10.1002/adfm.201902634.
2. Li, Z.; Zhang, Y.; Feng, N. Mesoporous silica nanoparticles: synthesis, classification, drug loading, pharmacokinetics, biocompatibility, and application in drug delivery. *Expert Opin. Drug Delivery* **2019**, *16*, 219-237, doi:10.1080/17425247.2019.1575806.
3. Li, T.; Shi, S.; Goel, S.; Shen, X.; Xie, X.; Chen, Z.; Zhang, H.; Li, S.; Qin, X.; Yang, H., et al. Recent advancements in mesoporous silica nanoparticles towards therapeutic applications for cancer. *Acta Biomater.* **2019**, *89*, 1-13, doi:10.1016/j.actbio.2019.02.031.

4. Castillo, R.R.; Lozano, D.; Gonzalez, B.; Manzano, M.; Izquierdo-Barba, I.; Vallet-Regi, M. Advances in mesoporous silica nanoparticles for targeted stimuli-responsive drug delivery: an update. *Expert Opin. Drug Delivery* **2019**, *16*, 415-439, doi:10.1080/17425247.2019.1598375.
5. Chinnathambi, S.; Tamanoi, F. Recent Development to Explore the Use of Biodegradable Periodic Mesoporous Organosilica (BPMO) Nanomaterials for Cancer Therapy. *Pharmaceutics* **2020**, *12*, 890.
6. Mai, N.X.D.; Nguyen, T.-H.T.; Vong, L.B.; Dang, M.-H.D.; Nguyen, T.T.T.; Nguyen, L.H.T.; Ta, H.K.T.; Nguyen, T.-H.; Phan, T.B.; Doan, T.L.H. Tailoring chemical compositions of biodegradable mesoporous organosilica nanoparticles for controlled slow release of chemotherapeutic drug. *Materials Science and Engineering: C* **2021**, *127*, 112232, doi:https://doi.org/10.1016/j.msec.2021.112232.
7. Guan, L.; Chen, J.; Tian, Z.; Zhu, M.; Bian, Y.; Zhu, Y. Mesoporous organosilica nanoparticles: Degradation strategies and application in tumor therapy. *VIEW* **2021**, *2*, 20200117, doi:https://doi.org/10.1002/VIW.20200117.
8. Guimarães, R.S.; Rodrigues, C.F.; Moreira, A.F.; Correia, I.J. Overview of stimuli-responsive mesoporous organosilica nanocarriers for drug delivery. *Pharmacol.. Res.* **2020**, *155*, 104742, doi:https://doi.org/10.1016/j.phrs.2020.104742.
9. Cheng, Y.; Jiao, X.; Fan, W.; Yang, Z.; Wen, Y.; Chen, X. Controllable synthesis of versatile mesoporous organosilica nanoparticles as precision cancer theranostics. *Biomaterials* **2020**, *256*, 120191, doi:https://doi.org/10.1016/j.biomaterials.2020.120191.
10. Yang, B.; Chen, Y.; Shi, J. Mesoporous silica/organosilica nanoparticles: Synthesis, biological effect and biomedical application. *Materials Science and Engineering: R: Reports* **2019**, *137*, 66-105, doi:https://doi.org/10.1016/j.mser.2019.01.001.
11. Yu, L.; Chen, Y.; Lin, H.; Du, W.; Chen, H.; Shi, J. Ultrasmall mesoporous organosilica nanoparticles: Morphology modulations and redox-responsive biodegradability for tumor-specific drug delivery. *Biomaterials* **2018**, *161*, 292-305, doi:https://doi.org/10.1016/j.biomaterials.2018.01.046.
12. Croissant, J.G.; Fatieiev, Y.; Almalik, A.; Khashab, N.M. Mesoporous Silica and Organosilica Nanoparticles: Physical Chemistry, Biosafety, Delivery Strategies, and Biomedical Applications. *Adv. Healthc. Mater.* **2018**, *7*, 1700831, doi:doi:10.1002/adhm.201700831.
13. Du, X.; Li, X.; Xiong, L.; Zhang, X.; Kleitz, F.; Qiao, S.Z. Mesoporous silica nanoparticles with organo-bridged silsesquioxane framework as innovative platforms for bioimaging and therapeutic agent delivery. *Biomaterials* **2016**, *91*, 90-127, doi:10.1016/j.biomaterials.2016.03.019.
14. Chen, Y.; Shi, J. Chemistry of Mesoporous Organosilica in Nanotechnology: Molecularly Organic-Inorganic Hybridization into Frameworks. *Adv. Mater.* **2016**, *28*, 3235-3272, doi:10.1002/adma.201505147.
15. Croissant, J.G.; Cattoen, X.; Wong Chi Man, M.; Durand, J.-O.; Khashab, N.M. Syntheses and applications of periodic mesoporous organosilica nanoparticles. *Nanoscale* **2015**, *7*, 20318-20334, doi:10.1039/c5nr05649g.
16. Yang, S.; Chen, S.; Fan, J.; Shang, T.; Huang, D.; Li, G. Novel mesoporous organosilica nanoparticles with ferrocene group for efficient removal of contaminants from wastewater. *J. Coll. Int. Sci.* **2019**, *554*, 565-571, doi:https://doi.org/10.1016/j.jcis.2019.07.037.
17. Hoffmann, F.; Cornelius, M.; Morell, J.; Froeba, M. Silica-based mesoporous organic-inorganic hybrid materials. *Angew. Chem., Int. Ed.* **2006**, *45*, 3216-3251.
18. Kickelbick, G. Hybrid inorganic-organic mesoporous materials. *Angew. Chem., Int. Ed.* **2004**, *43*, 3102-3104.
19. Tao, J.; Su, X.; Li, J.; Shi, W.; Teng, Z.; Wang, L. Intricately structured mesoporous organosilica nanoparticles: synthesis strategies and biomedical applications. *Biomaterials Science* **2021**, *9*, 1609-1626, doi:10.1039/D0BM02157A.
20. Wang, Y.; Zhang, B.; Ding, X.; Du, X. Dendritic mesoporous organosilica nanoparticles (DMONs): Chemical composition, structural architecture, and promising applications. *Nano Today* **2021**, *39*, 101231, doi:https://doi.org/10.1016/j.nantod.2021.101231.
21. Wang, Y.; Song, H.; Liu, C.; Zhang, Y.; Kong, Y.; Tang, J.; Yang, Y.; Yu, C. Confined growth of ZIF-8 in dendritic mesoporous organosilica nanoparticles as bioregulators for enhanced mRNA delivery in vivo. *National science review* **2021**, *8*, nwaa268, doi:10.1093/nsr/nwaa268.
22. Mezghrani, B.; Ali, L.M.A.; Richeter, S.; Durand, J.-O.; Hesemann, P.; Bettache, N. Periodic Mesoporous Ionosilica Nanoparticles for Green Light Photodynamic Therapy and Photochemical Internalization of siRNA. *ACS Appl. Mater. Interfaces.* **2021**, *13*, 29325-29339, doi:10.1021/acsami.1c05848.
23. Pham, T.C.; Nguyen, V.-N.; Choi, Y.; Lee, S.; Yoon, J. Recent Strategies to Develop Innovative Photosensitizers for Enhanced Photodynamic Therapy. *Chem. Rev.* **2021**, *121*, 13454-13619, doi:10.1021/acs.chemrev.1c00381.
24. Tsuboi, M.; Matsuo, K.; Ts'o, P.O.P. Interaction of poly-l-lysine and nucleic acids. *Journal of Molecular Biology* **1966**, *15*, 256-267, doi:https://doi.org/10.1016/S0022-2836(66)80225-5.
25. Daurat, M.; Rahmani, S.; Bouchal, R.; Akrout, A.; Budimir, J.; Nguyen, C.; Charnay, C.; Guari, Y.; Richeter, S.; Raehm, L., et al. Organosilica Nanoparticles for Gemcitabine Monophosphate Delivery in Cancer Cells. *ChemNanoMat* **2019**, *5*, 888-896, doi:https://doi.org/10.1002/cnma.201900202.
26. Aggad, D.; Mauriello Jimenez, C.; Dib, S.; Croissant, J.G.; Lichon, L.; Laurencin, D.; Richeter, S.; Maynadier, M.; Alsaiari, S.K.; Boufatit, M., et al. Gemcitabine Delivery and Photodynamic Therapy in Cancer Cells via

Porphyrin-Ethylene-Based Periodic Mesoporous Organosilica Nanoparticles. *ChemNanoMat* **2018**, *4*, 46-51, doi:10.1002/cnma.201700264.

27. Jimenez, C.M.; Rubio, Y.G.; Saunier, V.; Warther, D.; Stojanovic, V.; Raehm, L.; Frochot, C.; Arnoux, P.; Garcia, M.; Morère, A., et al. 20-nm-sized mesoporous silica nanoparticles with porphyrin photosensitizers for in vitro photodynamic therapy. *J. Sol-Gel Sci. Technol.* **2016**, *79*, 447-456, doi:10.1007/s10971-016-3991-6.
28. Yang, G.; Gong, H.; Qian, X.; Tan, P.; Li, Z.; Liu, T.; Liu, J.; Li, Y.; Liu, Z. Mesoporous silica nanorods intrinsically doped with photosensitizers as a multifunctional drug carrier for combination therapy of cancer. *Nano Research* **2015**, *8*, 751-764, doi:10.1007/s12274-014-0558-0.
29. Yang, Y.; Wan, J.; Niu, Y.; Gu, Z.; Zhang, J.; Yu, M.; Yu, C. Structure-Dependent and Glutathione-Responsive Biodegradable Dendritic Mesoporous Organosilica Nanoparticles for Safe Protein Delivery. *Chem. Mater.* **2016**, *28*, 9008-9016, doi:10.1021/acs.chemmater.6b03896.
30. Lacombe, S.; Cardy, H.; Simon, M.; Khoukh, A.; Soumillion, J.P.; Ayadim, M. Oxidation of sulfides and disulfides under electron transfer or singlet oxygen photosensitization using soluble or grafted sensitizers. *Photochem. Photobiol. Sci.* **2002**, *1*, 347-354, doi:10.1039/B202383K.
31. Samuelson Bannow, B.; Recht, M.; Négrier, C.; Hermans, C.; Berntorp, E.; Eichler, H.; Mancuso, M.E.; Klamroth, R.; O'Hara, J.; Santagostino, E., et al. Factor VIII: Long-established role in haemophilia A and emerging evidence beyond haemostasis. *Blood Reviews* **2019**, *35*, 43-50, doi:https://doi.org/10.1016/j.blre.2019.03.002.
32. Qu, J.; Ma, C.; Xu, X.-Q.; Xiao, M.; Zhang, J.; Li, D.; Liu, D.; Konkle, B.A.; Miao, C.H.; Li, L., et al. Comparative glycosylation mapping of plasma-derived and recombinant human factor VIII. *PLoS One* **2020**, *15*, e0233576, doi:10.1371/journal.pone.0233576.